Cent. Eur. J. Phys. • 9(2) • 2011 • 492-501
DOI: 10.2478/s11534-010-0095-8

VERSITA

Central European Journal of **Physics**

Symmetry and models of single-walled TiO_2 nanotubes with rectangular morphology*

Research Article

Robert A. Evarestov[1†], Yuri F. Zhukovskii[2], Andrei V. Bandura[1], Sergei Piskunov[2,3,4]

1 *Department of Quantum Chemistry, St. Petersburg State University, 26 Universitetsky Avenue, Petrodvorets 198504, Russia*

2 *Institute of Solid State Physics, University of Latvia, 8 Kengaraga Str., Riga LV-1063 Latvia*

3 *Faculty of Computing, University of Latvia, 19 Raina Blvd., Riga LV-1586, Latvia*

4 *Faculty of Physics and Mathematics, University of Latvia, 8 Zellu Str., Riga LV-1002, Latvia*

Received 3 August 2010; accepted 25 September 2010

Abstract: The formalism of line symmetry groups for one-periodic (1D) nanostructures with rotohelical symmetry has been applied for symmetry analysis of single-walled titania nanotubes (SW TiO_2 NTs) formed by rolling up the stoichiometric two-periodic (2D) slabs of anatase structure. Either six- or twelve-layer (101) slabs have been cut from TiO_2 crystal in a stable anatase phase. After structural optimization, the latter keeps the centered rectangular symmetry of initial slab slightly compressed along a direction coincided with large sides of elemental rectangles. We have considered two sets of SW TiO_2 NTs with optimized six- and twelve-layer structures, which possess chiralities $(-n, n)$ and (n, n) of anatase nanotubes. To analyze the structural and electronic properties of titania slabs and nanotubes, we have performed their *ab initio* LCAO calculations, using the hybrid Hartree-Fock/Kohn-Sham exchange-correlation functional PBE0. The band gaps ($\Delta\varepsilon_{gap}$) and strain energies (E_{strain}) of six-layer nanotubes have been computed and analyzed as functions of NT diameter (D_{NT}). As to models of 12-layer SW TiO_2 NTs of both chiralities, their optimization results in structural exfoliation, *i.e.*, the multi-walled structure should be rather formed in nanotubes with such a number of atomic layers.

PACS (2008): 61.46.Np, 61.48.De, 64.70.Nd, 73.22.-f

Keywords: line groups • rotohelical symmetry • TiO_2 nanotubes • anatase structure • hybrid HF-DFT PBE0 calculations

1. Introduction

As a well-known semiconductor with a numerous technological applications, titania is comprehensively studied in materials science [1]. The total number of TiO_2 polymorphs, discovered so far, is seven [2]. However, rutile and anatase undoubtedly prevail because of their higher stability as compared to other titania phases. Titania nanotubes (NTs) were systematically synthesized during the last 10-15 years using different methods and carefully studied as prospective technological materials [3–11]. Depending on the conditions of TiO_2 NTs synthesis, further XRD analysis identified their phase as either

*presented at the 6th International Conference on Functional Materials and Nanotechnologies, March 17-19, 2010, Riga, Latvia

†E-mail: re1973@re1973.spb.edu

anatase or rutile (the anatase phase was prevailing at temperatures below 450°C) [4]. In other experiments, the walls of synthesized TiO_2 nanotubes were described as a polycrystalline mixture of both anatase and rutile phases [5]. Two types of morphologies were observed in recently synthesized titania tubular nanostructures: cylindrical-like multi-walled (MW) and scroll-like, *e.g.*, containing various types of defects and impurities [3]. Their diameters usually vary from several to tens nm, with inter-wall distances ~ 0.5 nm and lengths up to several μm [7, 8]. Beyond the synthesis of pure titania nanotubes, a number of studies was performed for titanate nanosystems as possible precursors in the synthesis of TiO_2 NTs after thermal and chemical treatment [10]. They were also synthesized as layered nanotubes with structures of protonic lepidocrocite $H_xTi_{2-x/4}\square_{x/4}O_4$ ($\square$ indicates a Ti vacancy) [11] as well as polytitanic $H_2Ti_nO_{2n+1}$ acids and related alkali-containing compounds [6].

Since the growth mechanism for TiO_2 nanotubes is still not well defined, their comprehensive theoretical studies attract enhanced attention. In most theoretical simulations on titania nanotubes performed so far, a model 3D→2D→1D of structural transformations described in Ref. [12] was applied, *i.e.*, the bulk (3D) phase turns into a lamellar product (3D→2D), then the latter is bent and rolled to a single-walled (SW) nanotubular form (2D→1D). For 2D structure, a slab model of thermodynamically stable anatase TiO_2(101) surface [1] was mainly applied, which can be easily organized in double sub-sheets consisting of the two formula units with six-layer O-Ti-O_O-Ti-O structure with a centered rectangular morphology [13]. Nevertheless, the latter was very scarcely considered for simulation on TiO_2 NTs, during the last three years only [14–16], while a number of earlier and recent simulations on TiO_2 NTs were limited by triple-layered O-Ti-O structure, with optimization resulted in a hexagonal fluorite-like morphology [17–21]. This is not only due to computational limitations, *e.g.*, insufficient application of formalism of rotohelical symmetry in *ab initio* calculations, but also due to a presence of 3-layer fragments in structural units of separate walls in MW TiO_2 NTs [8]. As to anatase TiO_2(001) surface, it was found to be considerably less stable than (101) surface [1]. According to theoretical simulations [22, 23], the former can be reconstructed to a surface with lepidocrocite structure used for *ab initio* simulations on the corresponding TiO_2 nanotubes [17, 24]. Only SW TiO_2 NTs were simulated so far.

In this study, we continue theoretical study on titania nanotubes with anatase structure as considered previously [16]. In Section 2, we describe the line group symmetry of various TiO_2 nanotubes with centered rectangular morphology. A new approach to the generation of the line group irreducible representations is suggested, which is based on the isomorphism between line and plane groups. Section 3 describes computational details that used for calculations on TiO_2 sheets and nanotubes with centered rectangular (anatase) structure. In Section 4, we analyze the results calculated for 6- and 12-layer models of SW TiO_2 NTs with anatase morphology, systematize and discuss them. Section 5 summarizes the main conclusions obtained in this study.

2. Symmetry of TiO_2 single-walled nanotubes

The simplest description of the nanotube symmetry and structure is based on the so-called layer folding which means the construction of the cylindrical surfaces of nanotubes by rolling up the two-periodic (2D) crystalline layers (sheets and slabs).

The anatase TiO_2 bulk crystal is characterized by tetragonal space group 141 ($I4_1/amd$) with two formula units in the primitive unit cell (Table 1). We consider here three types of the nanotubes constructed from initial anatase slabs. The 3-layer model of the anatase (101) slab consists of three atomic layers (O-Ti-O), however, its structural optimization results in formation of fluorite-type (111) slab [17, 19] in which the symmetry can be attributed to the layer group 72 ($P\bar{3}m1$). It is the same for 3-layer slab with both anatase and fluorite structures, although the space symmetry of fluorite TiO_2 bulk crystal is described by cubic space group 225 ($Fm\bar{3}m$). In the case of 6-layer model (O_O-Ti_Ti-O_O), all the six atoms of the bulk primitive unit cell are included. The 12-layer (O_O-Ti_Ti-O_O_O_O-Ti_Ti-O_O) model contains the two quasi-separated 6-layer slabs. The layer group 18 ($C2/m11$ with a centered rectangular lattice) describes the symmetry of both 6- and 12-layer slabs. Bulk titania with lepidocrocite structure can be attributed to the orthorhombic space group 63 ($Cmcm$). The 6-layer model of the lepidocrocite (010) slab consists of six atomic layers (O-Ti-O_O-Ti-O) [24]. The layer group 46 ($Pmmn$ with primitive rectangular lattice) describes its symmetry.

Let **a** and **b** be the primitive translation vectors of the two-periodic (2D) lattice of the layer and γ the angle between them. To specify the symmetry of nanotubes as monoperiodic (1D) systems, it is necessary to define a finite 1D translation vector $\mathbf{L} = l_1\mathbf{a} + l_2\mathbf{b}$ along the nanotube axis and normal to the chiral vector $\mathbf{R} = n_1\mathbf{a} + n_2\mathbf{b}$, ($l_1$, l_2, n_1 and n_2 are integers). The nanotube of the chirality (n_1, n_2) is obtained by folding the layer in a way that the chiral vector **R** becomes circumference of the tube.

Table 1. Line symmetry groups of SW TiO_2 NTs, rolled from two periodic titania layers.

Object	Space group	layer	Layer group	Line groups for special chiralities[a]	P_i	Line groups for general chiralities (n_1,n_2)
3-layer hexagonal	225 $Fm\bar{3}m$	(111)	72 ($P\bar{3}m1$)	4h $(2n)_n/m$ 8g $(2n)_n mc$	C_{2nh} C_{2nv}	$1\,n_q(C_q)$
6-layer centered rectangular	141 $I4_1/amd$	(101)	18 ($C2/m11$)	4e $(2n)_n/m$ 8d $(2n)_n mc$	C_{2nh} C_{2nv}	$1\,n_q(C_q)$
12-layer centered rectangular	141 $I4_1/amd$	(101)	18 ($C2/m11$)	4e $(2n)_n/m$ 8d $(2n)_n mc$	C_{2nh} C_{2nv}	$1\,n_q(C_q)$
6-layer primitive rectangular	63 $Cmcm$	(010)	46 ($Pmmn$)	11c n/mmm^b $(\bar{2}n)2m^c$	D_{nh}	$5\,n_q\,22(D_q)$

[a]special chiralities: c - $(n,0)$, $(0,n)$; d - (n,n); e - $(-n,n)$; g - $(n,0)$, $(0,n)$, $(-n,n)$; h - (n,n), $(-n,2n)$, $(-2n,n)$;
i - $(n,0)$, $(0,n)$, $(-n,n)$, (n,n), $(-n,2n)$, $(-2n,n)$
[b]for even n
[c]for odd n

The orthogonal vectors **R** and **L** are connected with the 2D lattice translation vectors **a** and **b** by the transformation

$$\begin{pmatrix} \mathbf{R} \\ \mathbf{L} \end{pmatrix} = \mathrm{Q} \begin{pmatrix} \mathbf{a} \\ \mathbf{b} \end{pmatrix}.$$

The determinant

$$q = \begin{vmatrix} n_1 & n_2 \\ l_1 & l_2 \end{vmatrix}$$

of the matrix

$$\mathrm{Q} = \begin{pmatrix} n_1 & n_2 \\ l_1 & l_2 \end{pmatrix}$$

is equal to the number of 2D lattice points in the 2D-supercell formed by the chiral **R** and translation **L** vectors. The orthogonality relation $(\mathbf{RL}) = 0$ can be written in the form:

$$\frac{l_1}{l_2} = -\frac{n_2 a^2 + n_1 ab\cos\gamma}{n_1 b^2 + n_2 ab\cos\gamma}, \qquad (1)$$

where $a = |\mathbf{a}|$ and $b = |\mathbf{b}|$.

The symmetry of nanotube is defined by: (*i*) nanotube chirality (n_1, n_2), (*ii*) translation vector components (l_1, l_2) found from the orthogonality relation, Eq. (2), (*iii*) point symmetry of the rolled 2D lattice (see below).

The orthogonality relation is realized in different forms for different 2D lattices. For the hexagonal and rectangular lattices, this relation (1) is transformed to hexagonal $(\cos\gamma = 0.5; a = b)$:

$$\frac{l_1}{l_2} = -\frac{2n_2 + n_1}{2n_1 + n_2}, \qquad (2)$$

rectangular centered $(\cos\gamma \neq 0, 0.5; a = b)$:

$$\frac{l_1}{l_2} = -\frac{n_2 + n_1\cos\gamma}{n_1 + n_2\cos\gamma}, \qquad (3)$$

rectangular primitive $(\cos\gamma = 0; a \neq b)$:

$$\frac{l_1}{l_2} = -\frac{n_2 a^2}{n_1 b^2}, \quad \text{or} \quad l_1 n_1 b^2 = -l_2 n_2 a^2. \qquad (4)$$

It is well seen from Eqs. (2)-(4) that the translational symmetry of the nanotube may exist for any arbitrary chirality (n_1, n_2) if the nanotube is obtained by folding the layer with hexagonal 2D lattices. However, there are restrictions on the chiralities for rectangular lattices: $(n, 0)$, $(0, n)$ for rectangular primitive and $(-n, n)$, (n, n) for rectangular centered ones. These chiralities are known as special chiralities and are given in column 5 of Table 1. The chiralities $(n, 0)$ and $(0, m)$ introduced earlier in [14–16] for description of 6-layer anatase-type TiO_2 nanotubes (where formalism of rotohelical symmetry was not yet applied) correspond to chiralities $(-n, n)$ and (n, n) used in the present study. Both former chiralities refer to the rectangular primitive lattice described by Eq. (4).

The translations of the layer become rotohelical operations T_q^r on the nanotube, giving the first family subgroup $1\,n_q$ of the NT line group L (Table 1). The latter has the same parameters for the ray of the nanotubes $(n_1, n_2) = n(\tilde{n}_1, \tilde{n}_2)$, differing by n.

Apart from the translational invariance, the layer groups have rotational symmetry generated by the rotations around the axis perpendicular to the layer. But after the layer rolling only the second order axis U survives, being compatible with the monoperiodic symmetry. In addition,

the non-oblique 2D lattices have both vertical mirror and glide planes, but not all of them continue to be symmetric operations for nanotubes. Thirteen families of line groups L are known [25, 26]. In column 5 of Table 1, the number of line group families is given with the special chiralities and factor group $P_i = \frac{L}{T}$, where T is the group of one-dimensional translations along the tube axis.

3. Computation details

The first principles LCAO (Linear Combination of Atomic Orbitals) calculations of various titania sheets and nanotubes have been performed using the hybrid HF-KS (PBE0) exchange-correlation functional [27, 28] as implemented in *CRYSTAL-06*[1] code. The small-core pseudopotential [29] of Ti atom is used in titania nanotube calculations ($3s, 3p, 3d$ and $4s$-electrons were taken as valence electrons), while the all-electron BS for O-atom has been taken from Ref. [30]. It is well known that in the LCAO calculations of crystals the BS of free atom has to be modified as the diffuse functions cause numerical problems because of the large overlap with the core functions of the neighboring atoms in a dense-packed crystal [31].

There exist a number of different algorithms for minimization of many-variable functions [32]. The comparative study of their efficiency for the basis set optimization in crystals has been performed recently [33]. To optimize the BS in present study, we use the minimization method without calculations on the total energy derivatives developed by Powell [34] and often called 'the method of conjugate directions'. It is estimated as one of the most efficient direct minimization methods. Being interfaced with the *CRYSTAL06* LCAO computational code[1] our program package *OPTBAS* [33] has been applied for the BS optimization. The BS exponential parameters less than 0.1 were excluded from the AOs and the bound-constrained optimization has been performed for the remaining exponential parameters with a 0.1 lower bound.

The diffuse exponents of valence s, p and d-orbitals have been optimized for stable anatase phase of bulk titania. Its atomic and electronic properties have been reproduced in good agreement with the experiment (the experimental values are given in brackets): the lattice parameters $a = 3.784$ Å (3.782 Å) and $c = 9.508$ Å (9.502 Å), the dimensionless parameter for relative position of oxygen atom $u = 0.2074$ (0.2080), although the reproduced values of $\Delta\varepsilon_{gap}$ are worse, being overestimated: 4.0 eV *vs.* 3.2 eV. In any case, these results for the bulk titania (anatase) agree with the experimental data better than those given in [35] for both plane wave (PW) and LCAO calculations when using the different exchange-correlation potentials. Certain improvement of substantially underestimated values of $\Delta\varepsilon_{gap}$ for bulk anatase in the DFT PW calculations was achieved recently [21] when using the LDA+U method (2.7 eV).

The monoperiodic translation symmetry has been adopted for our nanotube calculations as it was implemented with POLYMER option in *CRYSTAL06*[1] code. Unfortunately, this option takes into account only the symmetry of rod groups being the subset of the nanotube line groups as present in Table 1. Serious attempt to overcome this difficulty has been undertaken recently: the last release of *CRYSTAL* package[2] contains a special input option which allows generation of 1D nanotubes from 2D slabs. However, the formalism of line groups has not been implemented in *CRYSTAL09*code.

4. Structural and electronic properties of TiO_2 slabs and nanotubes

4.1. 6- and 12-layer titania sheets with initial anatase (101) structure

TiO_2 sheets with a thickness of a few atomic layers were found to be remarkably stable [23]. In the present study, we have optimized the structures of 6- and 12-layer anatase (101) slabs (Fig. 1) cut from anatase bulk as well as calculated their properties. Both 6- and 12-layer anatase (101) slabs keep initial symmetry (Table 1) after structural optimization, although their lattice parameters differ from those in bulk, especially c (Table 2). Both six- and twelve-layer slabs expose five-fold coordinated titanium atoms, while oxygen atoms can be both two- and three-fold coordinated (Fig. 2).

[1] R. Dovesi, V.R. Saunders, C. Roetti, R. Orlando, C.M. Zicovich-Wilson, F. Pascale, B. Civalleri, K. Doll, N.M. Harrison, I.J. Bush, Ph. D'Arco, M. Llunell, CRYSTAL-2006 User Manual (University of Turin, 2006)

[2] R. Dovesi, V.R. Saunders, C. Roetti, R. Orlando, C.M. Zicovich-Wilson, F. Pascale, B. Civalleri, K. Doll, N.M. Harrison, I.J. Bush, Ph. D'Arco, M. Llunell, CRYSTAL-2009 User Manual (University of Turin, 2010), http://www.crystal.unito.it

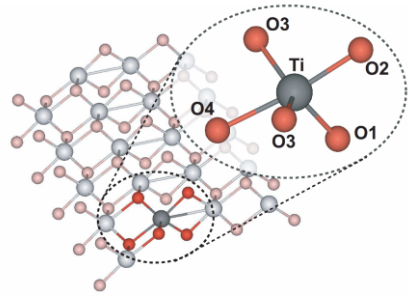

Figure 1. Five-fold coordination for Ti atoms in six-layer centered rectangular titania sheets.

Surface and formation energies of both titania slabs are qualitatively similar to those calculated earlier [13, 21, 23]: the former grew when increasing the thickness of slab, and the latter reduced. Results presented in Table 2 also indicate a certain convergence of titania sheet properties to bulk ones with increasing of slab thickness. Image of cross-section for 12-layer TiO_2 sheet (Fig. 2b) shows no noticeable structural change unlike the same for 6-layer titania slab. When comparing $\Delta\varepsilon_{gap}$ for 6- and 12-layer slabs (Table 2) we can conclude that when increasing a thickness of titania sheet, the band gap should approach to the value of anatase bulk.

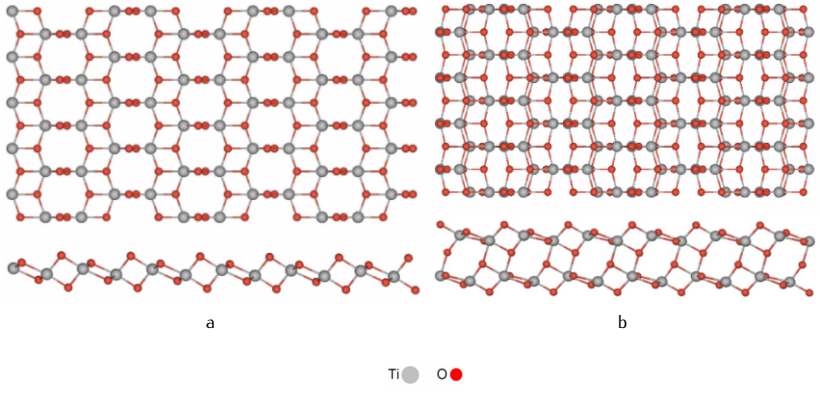

Figure 2. Models of stoichiometric (101) titania sheets of different thickness optimized from the corresponding slabs with initial geometry of bulk anatase (atop and across images): (a) 6-layer slab (thickness 0.24 nm); (b) 12-layer slab (thickness 0.58 nm).

Table 2. The atomic and electronic structure of TiO_2 bulk *vs.* various slabs (Figs. 1, 2).

models of TiO_2 bulk and sheets	lattice parameters, (Å)		thickness h_{NT}, (Å)	bond length $d_{Ti\text{-}O}$[a], (Å)				effective charge q_{Ti}[b], *e*	E_{relax} *per* TiO_2 unit[c], eV	surface energy E_{surf}[d], J/m^2	$\Delta\varepsilon_{gap}$[e], eV
	a	*c*		Ti-O1	Ti-O2	Ti-O3	Ti-O4				
bulk	3.78	9.51	-	1.935	1.935	1.973	1.973	2.35	-	-	4.09
6-layer	3.51	5.45	2.39	1.75	1.89	1.91	2.05	2.28	-1.09	0.64	5.14
12-layer	3.71	5.46	5.83	1.77	1.83	1.95	2.01	2.30	-0.55	0.67	4.92

[a] the corresponding bonds are shown in Fig. 1
[b] averaged effective charges q_O are as twice as smaller than q_{Ti}, with opposite sign
[c] E_{relax} is a difference of energies between slab with "bulk" geometry and that with optimized structure
[d] $E_{surf}(n) = \frac{1}{2S}(E_n - nE_b)$, where E_n is the total energy of *n*-layer slab *per* primitive surface unit cell, *S* its area, while E_b the total energy *per* primitive bulk unit cell
[e] all band gaps considered in this Table are indirect

4.2. Six- and twelve-layer single-walled TiO_2 nanotubes

The six-layer titania sheets with anatase-type (101) structure can be rolled up to 6-layer titania SW NTs with (*i*) $(-n, n)$ chirality and (*ii*) (n, n) chirality. Fig. 3 shows the optimized structures of the selected 6-layer nanotubes of both chiralities. A specific feature of these six-layer titania sheets and nanotubes is that both Ti sublayers are rearranged in the middle between both surfaces of the sheets and nanotubes (Figs. 2a and 3), *i.e.*, their optimized structure O_O-Ti_Ti-O-O differs from O-Ti-O_O-Ti-O according to a sequence of TiO_2 formula units in the bulk anatase structure.

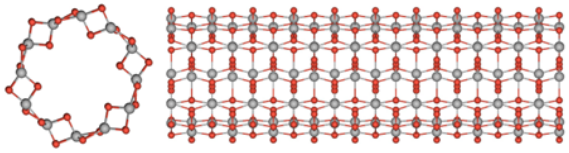

a across and aside images of optimized 6-layer $(-3, 3)$ TiO_2 nanotube with a [010] orientation of axis and $D_{NT} = 1.00$ nm.

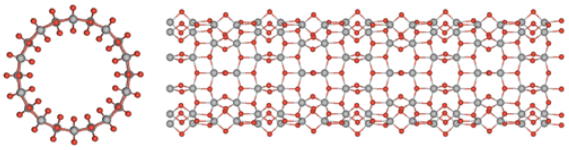

b across and aside images of optimized 6-layer $(10, 10)$ TiO_2 nanotube with a $[\bar{1}01]$ orientation of axis and $D_{NT} = 1.18$ nm.

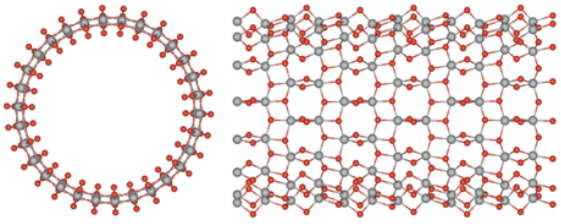

c across and aside images of optimized 6-layer $(15, 15)$ TiO_2 nanotube with a $[\bar{1}01]$ orientation of axis and $D_{NT} = 1.73$ nm.

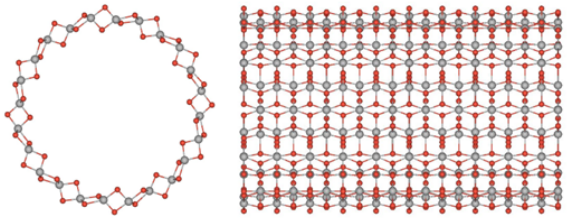

d across and aside images of optimized 6-layer $(-6, 6)$ TiO_2 nanotube with a [010] orientation of axis and $D_{NT} = 1.98$ nm.

Figure 3. Four 6-layer anatase-like SW TiO_2 nanotubes with different chiralities and diameters.

In Table 3, we present results obtained after structural optimization of 6-layer TiO_2 NTs with (*i*) $(-n, n)$ chirality (for $n = 3, 4, 6, 9, 12$) and (*ii*) (n, n) chirality (for $n = 6, 10, 15, 20, 24$). One of the main parameters of nanotube stability, *i.e.*, the strain energy E_{strain}, is defined as the difference between the total energies of the optimized nanotube (E_{NT}) and the corresponding slab before rolling up (E_{slab}), taking into account the number k of slab unit cells in nanotube unit cell containing m formula units TiO_2 (measured in kJ/mol *per* TiO_2 formula unit):

$$E_{strain} = \frac{1}{m}\left(E_{NT} - kE_{slab}\right). \qquad (5)$$

Obviously, the number of atoms *per* surface unit in $(-n, n)$ nanotubes is markedly smaller than that in (n, n) NTs of the same diameter, thus, the latter can be calculated faster. For a small D_{NT} (low chirality indices), the absolute values of both E_{relax} and E_{strain} are large enough, and trying to reduce these diameters even more, we face an enhanced instability of NTs. For example, the convergence of calculations on $(4, 4)$ nanotubes has been found to be rather poor. Since hypothetical nanotubes with infinite diameter should coincide with sheets of the same thickness, a consequent growth of the NT diameters leads to a substantial decrease of both relaxation and strain energies (down to zero at infinity), whereas the values of $h_{NT}, d_{Ti\text{-}O}, q_{Ti}$ and $\Delta\varepsilon_{gap}$ (Table 3) approach to those for 6-layer titania slab with a hexagonal structure (Table 2).

We also analyze dependence of E_{strain} and $\Delta\varepsilon_{gap}$ on D_{NT} for six-layer TiO_2 NTs simulated in present study (Figs. 4 and 5, respectively). We have considered a large enough range of nanotube diameters, from 0.5 nm to 4.0 nm, with a number of atoms *per* NT unit cell increased from 36 up to 288. To construct both plots on Figs. 4 and 5, we have performed calculations with the total geometry optimization for altogether 12 one-periodic models of SW TiO_2 NTs of different morphologies.

Table 3. The structural and electronic properties of the six-layer SW TiO_2 NTs (Fig. 3)[a].

NT chirality indices	N_a	l_{NT}[b], Å	D_{NT}[c], Å	h_{NT}, Å	d_{Ti-O}, Å (Fig. 1)				q_{Ti}, e	E_{relax}, eV/TiO_2	E_{strain}, kJ/mol *per* TiO_2	$\Delta\varepsilon_{gap}$[d], eV
					Ti-O1	Ti-O2	Ti-O3	Ti-O4				
$(-n,n)$ nanotubes - $(2n)_n/m$ group												
(−3, 3)	36	3.66	9.98	2.45	1.795	1.86	1.925	2.025	2.28	-0.82	16.86	4.92 (i)
(-4,4)	48	3.60	13.30	2.41	1.775	1.89	1.94	2.01	2.21	-0.35	12.20	5.40 (i)
(-6,6)	72	3.54	19.84	2.39	1.765	1.87	1.92	2.11	2.19	-0.14	6.47	5.26 (i)
(-9,9)	108	3.52	29.68	2.39	1.77	1.875	1.91	2.09	2.27	-0.05	4.57	5.19 (i)
(-12,12)	144	3.52	39.55	2.39	1.77	1.88	1.90	2.085	2.27	-0.03	3.20	5.17 (i)
(n,n) nanotubes - $(2n)_nmc$ group												
(6,6)	72	10.32	7.22	2.44	1.79	1.835	1.96	2.01	2.27	-1.68	34.54	4.76 (d)
(10,10)	120	10.39	11.85	2.46	1.80	1.835	1.945	2.02	2.27	-0.45	18.39	5.05 (d)
(15,15)	180	10.33	17.33	2.43	1.785	1.87	1.92	2.01	2.27	-0.14	12.25	5.36 (i)
(20,20)	240	10.33	22.84	2.41	1.78	1.875	1.91	2.01	2.28	-0.07	8.51	5.28 (d)
(24,24)	288	10.33	27.24	2.41	1.78	1.875	1.895	2.01	2.28	-0.03	6.57	5.24 (d)

[a] definition of the most of values is the same as in Table 2
[b] length of nanotube unit cell
[c] diameters are given for the middle cylinders between the external and internal walls of NTs
[d] direct and indirect band gaps are marked by superscript indices (d) and (i), respectively

Two curves $E_{strain}(D_{NT})$ imaged in Fig. 4 show that the strain energy of six-layer NTs with $(-n,n)$ chirality is smaller than that for (n,n) NTs of a similar diameter, *i.e.*, the former are more stable energetically. This difference remains noticeable for nanotubes with diameters $\leqslant$ 30 Å. When diameters of nanotubes increase up to 40 Å the strain energies decrease and approach each other.

For six-layer titania nanotubes of both chiralities, $\Delta\varepsilon_{gap}(D_{NT})$ curves possess maxima at diameter range 13-17 Å (Fig. 5). For larger values of D_{NT}, both the relaxation and strained energies of TiO_2 nanotubes substantially decrease while their band gaps asymptotically approach to that for the corresponding 2D slab (Table 2). We observe some discrepancy with the corresponding results obtained in Ref. [14] (where the authors obtain a relief for the curves $\Delta\varepsilon_{gap}(D_{NT})$ qualitatively similar to changes of the band gap calculated for the hexagonal 3-layer titania nanotubes [21] where $\Delta\varepsilon_{gap}$ is permanently growing). However, results obtained using the method of empirical potentials [14] cannot be properly compared with results of our *ab initio* calculations.

We also have tried to simulate the twelve-layer single-walled TiO_2 nanotubes with the anatase morphology. The middle of the 12-layer TiO_2 slab described in Subsection 4.1 consists of two sublayers containing oxygen atoms (Fig. 2b), and when we obtain the single-walled titania nanotube by rolling up this twelve-layer sheet its thickness is about 2.5 times larger than that for six-layer TiO_2 nanotube. As a result, the atomic structure of the internal wall surface of this 12-layer NT is overstrained

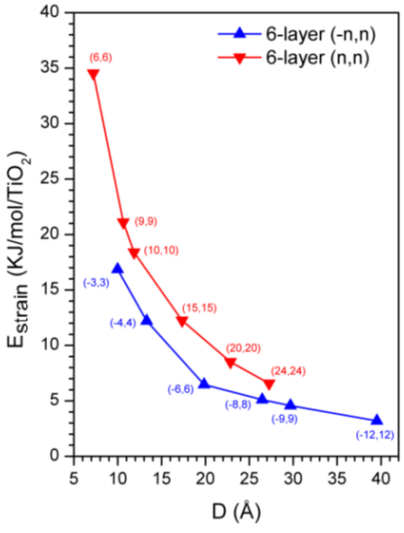

Figure 4. Strain energies E_{strain} *vs.* D_{NT} for the two sets of six-layer SW TiO_2 NTs with various chiralities.

even for moderate values of D_{NT}. A comparison of images for both six- and twelve-layer NTs with the same $(-6,6)$ and $(12,12)$ chiralities (Fig. 5) clearly shows quite small geometry relaxation of the former and drastic change of morphology of the latter which cannot be optimized at all, due to a divergence of the SCF calculations after several steps of geometry optimization.

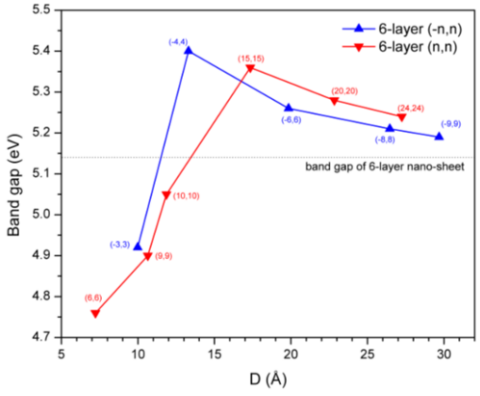

Figure 5. Band gaps $\Delta\varepsilon_{gap}$ *vs.* D_{NT} for the two sets of six-layer SW TiO_2 NTs with various chiralities.

This instability can be also illustrated by a drastic difference between the calculated strain energies (E_{strain}) of 6- and 12-layer SW TiO_2 NTs with the non-optimized structure after rolling up the corresponding slabs (Fig. 2) in the case of $(-6, 6)$ and $(12, 12)$ chiralities: 23.76 and 41.78 *vs.* 224.04 and 498.62 kJ/mol *per* TiO_2 formula unit, respectively. Thus, we can predict that for 12-layer titania nanotubes, the more stable morphology has not to be the exfoliating SW NT but the double-walled (DW) NT containing a pair of the separated six-layer nanotubes of different diameters and chirality indices.

(-6,6) chirality		(12,12) chirality	
6-layer NTs	12-layer NTs	6-layer NTs	12-layer NTs
Initial morphology of nanotubes			
D_{NT}= 19.33 Å	D_{NT}= 19.67 Å	D_{NT}= 12.99 Å	D_{NT}= 14.13 Å
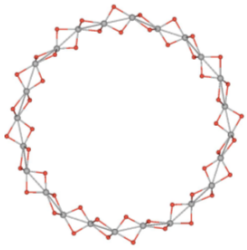	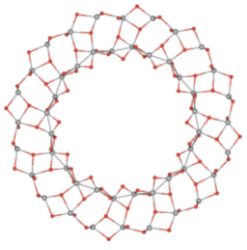	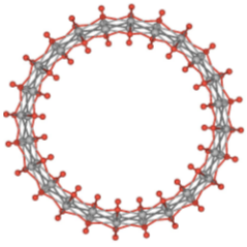	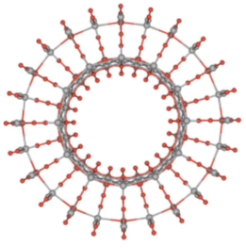
Nanotube morphology after complete (6-layer NTs) and partial (12-layer NTs) optimization			
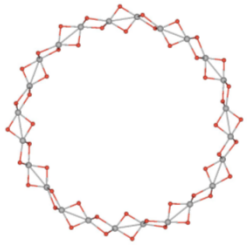	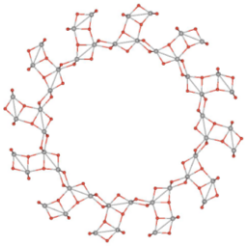	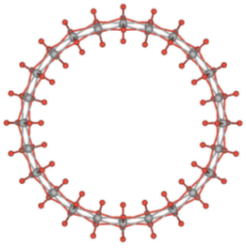	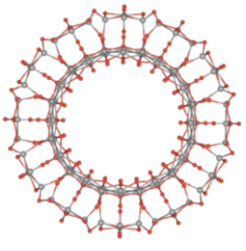

Figure 6. Cross-sections of 6- and 12-layer SW TiO_2 NTs with $(-6, 6)$ and $(12, 12)$ chiralities, respectively (D_{NT} for nanotubes with initial geometry are defined as described in Table 3).

5. Conclusions

1. Use of the line group formalism allows the construction of nanotubes of different crystalline morphology. The exploitation of the rotohelical symmetry of NTs, usually quite high, permits to drastically reduce the computation time. A new approach is suggested for the generation of the line group irreducible representations. This approach is based on the isomorphism between line and plane groups.

2. *Ab initio* LCAO calculations using the hybrid PBE0 Hamiltonian allow us to perform the analysis of the atomic and electronic structure of TiO_2 sheets as well as nanotubes simulated using different models.

3. The strain energies of 6-layer SW TiO_2 NTs decrease with the growth of nanotube diameter, approaching to a minimum for infinite D_{NT}. $\Delta\varepsilon_{gap}(D_{NT})$ curves for both nanotube chiralities achieve maxima at diameter range 13-17 Å and after its further growth both gaps asymptotically approach to that for the corresponding 2D slab.

4. The twelve-layer SW TiO_2 NTs have been found to be energetically non-stable as single-walled nanotubes. We can predict that for these nanotubes, the more preferable morphology has to be double-walled (DW) NTs of the same chirality consisting of a pair of six-layer nanotubes of different diameters and chirality indices.

Acknowledgement

R.E. is grateful to Prof. M. Damnjanovi_ for stimulating discussions, S.P. is thankful for the financial support through the ESF project Nr. 2009/0216/1DP/1.1.1.2.0/09/APIA/VIAA/044.
The authors thank M.V. Losev for essential contribution in development of computational formalism used in this study.

References

[1] U. Diebold, Surf. Sci. Rep. 48, 53 (2003)
[2] J. Muscat, V. Swamy, N.M. Harrison, Phys. Rev. B 65, 224112 (2002)
[3] W. Wang, O.K. Varghese, M. Paulose, C.A. Grimes, J. Mater. Res. 19, 417 (2004)
[4] J. Zhao, X. Wang, T. Sun, L. Li, Nanotechnology 16, 2450 (2005)
[5] T. Maiyalagan, B. Viswanathan, U.V. Varadaraju, Bull. Mater. Sci. 29, 705 (2006)
[6] D.V. Bavykin, J.M. Friedrich, F.C. Walsh, Adv. Mater. 18, 2807 (2006)
[7] N. Viriya-empikul, N. Sano, T. Charinpanitkul, T. Kikuchi, W. Tanthapanichakoon, Nanotechnology 19, 035601 (2008)
[8] G. Mogilevsky, Q. Chen, A. Kleinhammes, Y. Wu, Chem. Phys. Lett. 460, 517 (2008)
[9] R. Tenne, G. Seifert, Ann. Rev. Mater. Res. 39, 387 (2009)
[10] S. Zhang et al., Phys. Rev. Lett. 91, 256103 (2003)
[11] R. Ma, Y. Bando, T. Sasaki, Chem. Phys. Lett. 380, 577 (2003)
[12] Y.Q. Wang, C.G. Hu, X.F. Duan, H.L. Sun, Q.K. Hue, Chem. Phys. Lett. 365, 427 (2002)
[13] W. Hebenstreit, N. Ruzycki, G.S. Herman, Y. Gao, U. Diebold, Phys. Rev. B 62, R16334 (2000)
[14] Z. Liu, Q. Zhang, L.C. Qin, Solid State Commun. 141, 168 (2007)
[15] F. Lin et al., Chem. Phys. Lett. 475, 82 (2009)
[16] A.V. Bandura, R.A. Evarestov, Surf. Sci. 603, L117 (2009)
[17] A.N. Enyashin, G. Seifert, Phys. Status Solidi B 242, 1361 (2005)
[18] A.N. Enyashin, A.L. Ivanovskii, J. Mol. Struct.: THEOCHEM 766, 15 (2006)
[19] J. Wang et al., Physica E 41, 838 (2009)
[20] D.J. Mowbray, J.I. Martinez, J.M. García Lastra, K.S. Thygesen, K.W. Jacobsen, J. Phys. Chem. C 113, 12301 (2009)
[21] T. He et al., J. Phys. Chem. C 113, 13610 (2009)
[22] F. Alvarez-Ramirez, Y. Ruiz-Morales, Chem. Mater. 19, 2947 (2007)
[23] A. Vittadini, M. Casarin, Theor. Chem. Acc. 120, 551 (2008)
[24] D. Szieberth, A.M. Ferrari, Y. Noel, M. Ferrabone, Nanoscale 2, 81 (2010)
[25] M. Vujičić, J. Phys. A: Math. Gen. 10, 1271 (1977)
[26] M. Damnjanović, I. Milošević, Line Groups in Physics: Theory and Applications to Nanotubes and Polymers, Lecture Notes in Physics, Vol. 801 (Springer Verlag, Berlin, Heidelberg, 2010)
[27] M. Ernzerhof, G.E. Scuseria, J. Chem. Phys. 110, 5029 (1999)
[28] C. Adamo, V. Barone, J. Chem. Phys. 110, 6158 (1999)
[29] M.M. Hurley, L.F. Pacios, P.A. Christiansen, R.B. Ross, W.C. Ermler, J. Chem. Phys. 84, 6840 (1986)
[30] A. Schäfer, C. Huber, R. Ahlrichs, J. Chem. Phys. 100, 5829 (1994)
[31] R.A. Evarestov, Quantum Chemistry of Solids. The LCAO First Principles Treatment of Crystals,

Springer Series in Solid State Sciences, Vol. 153 (Springer Verlag, Berlin, 2007)
[32] B.D. Bunday, Basic Optimization Methods (Edward Arnold Ltd., London, 1984)
[33] R.A. Evarestov, A.I. Panin, A.V. Bandura, M.V. Losev, J. Phys. Conf. Ser. 117, 012015 (2008)
[34] W.H. Press, S.A. Teukolski, W.T. Vetterling, B.P. Flannery, Numerical Recipes in FORTRAN 77: The Art of Scientific Computing, Vol. 1, 3rd Ed. (Cambridge University Press, New York, 2007)
[35] F. Labat, P. Baranek, C. Domain, C. Minot, C. Adamo, J. Chem. Phys. 126, 154703 (2007)